Time-Optimal Trajectories to Circumsolar Space Using Solar Electric Propulsion

Alessandro A. Quarta,[a,*] Dario Izzo[b] and Massimiliano Vasile[c]

[a] *Dipartimento di Ingegneria Aerospaziale, University of Pisa, I-56122 Pisa, Italy*

[b] *Advanced Concepts Team, European Space Agency, Noordwijk, The Netherlands*

[c] *Department of Mechanical Engineering, University of Strathclyde, Glasgow, UK*

Abstract

The aim of this paper is to explore the capabilities of a solar electric propelled spacecraft on a mission towards circumsolar space. Using an indirect approach, the paper investigates minimum time of transfer (direct) trajectories from an initial heliocentric parking orbit to a desired final heliocentric target orbit, with a low perihelion radius and a high orbital inclination. The simulation results are then collected into graphs and tables for a trade-off analysis of the main mission parameters.

Key words: Minimum time trajectories, Solar electric propulsion, Circumsolar space exploration

* Corresponding author.

Email addresses: a.quarta@ing.unipi.it (Alessandro A. Quarta,), dario.izzo@esa.int (Dario Izzo), massimiliano.vasile@strath.ac.uk (Massimiliano Vasile).

Nomenclature

$\mathbb{A}$	=	matrix $\in \mathbb{R}^{7\times 3}$, see Eq. (A.2)
a	=	semimajor axis [AU]
$\hat{\boldsymbol{a}}_T$	=	propulsive acceleration unit vector
$\boldsymbol{d}$	=	vector $\in \mathbb{R}^{7\times 1}$, see Eq. (A.3)
e	=	orbital eccentricity
f, g, h, k	=	modified equinoctial elements
H	=	Hamiltonian function
i	=	orbital inclination [deg]
I_d	=	thruster operation point
J	=	performance index
L	=	true longitude [deg]
m	=	spacecraft mass [kg]
m_p	=	propellant mass [kg]
P	=	input power to Power Processing Unit [W]
P_L	=	payload power [W]
$P_\oplus$	=	solar array initial output power [W]
p	=	semilatus rectum [AU]
r	=	Sun-spacecraft distance [AU]
r_a	=	target orbit's aphelion radius [AU]
r_p	=	target orbit's perihelion radius [AU]
T	=	propulsive thrust [N]
t	=	time [days]
$\boldsymbol{x}$	=	state vector
β	=	propellant mass flow rate [mg/s]

δ	=	ecliptic declination [deg]
η_P	=	duty cycle
$\boldsymbol{\lambda}$	=	adjoint vector
λ	=	adjoint variable
$\mu_\odot$	=	Sun's gravitational parameter [km^3/s^2]
ν	=	true anomaly [deg]
ω	=	argument of perihelion [deg]
Ω	=	right ascension of the ascending node [deg]

Subscripts

0	=	initial, parking orbit
1	=	final, target orbit

Superscripts

$\cdot$	=	time derivative

1 Introduction

The circumsolar space, with particular reference to the region around the Sun's poles, is still, to a large extent, an unexplored part of our Solar System. Despite a continuous progress of remote sensing capabilities, a~~n~~ deep knowledge of the inner heliosphere can be obtained only through accurate in-situ measurements [1]. In fact an in-depth analysis of the solar wind or

a thorough measurement of the solar magnetic field, and of its interaction with the external corona, requires the use (in situ) of a scientific probe. Even more interesting is the possibility to observe the Sun at high inclinations above the Ecliptic plane.

The interest of the scientific community for exploring the circumsolar space has been revived after the remarkable results of the Ulysses mission, including the observation of an unexplained constant decrease of the solar wind since the beginning of space based recordings, and further confirmed by the launch of the European probe Solar Orbiter [2], which is scheduled for the beginning of 2017. Its operating orbit is characterized by a perihelion distance of about 0.28 AU and an inclination greater than 25 deg with respect to the solar equatorial plane. Such a probe is expected to provide detailed information both of the inner heliosphere and of the solar polar regions. A closer view of the Sun will be given by the American Solar Probe Plus [3], whose launch will take place on 2018. The Solar Probe Plus should be the first spacecraft capable of traveling within the solar atmosphere (the solar corona) and reaching a distance of 5.9 million kilometers (that is, 8.5 solar radii) from the photosphere, the region from which the photons originate.

The difficulty of reaching the circumsolar space with a scientific probe comes from the high ΔV necessary for those mission types. In fact, the desired scientific measurements typically require the achievement of a heliocentric orbit with a low perihelion and a high inclination with respect to the Ecliptic plane. For example, a circular orbit with a radius of 0.28 AU and an inclination of 28 deg with respect to the Ecliptic plane would require a minimum $\Delta V \simeq 29$ km/s using a two impulse maneuver. Such a value could be reduced, the perihelion distance and inclination being the same, using an elliptic orbit. In fact, with an aphelion radius of 0.8 AU the ΔV decreases to about 17.2 km/s. The Ulysses mission, one of the very first missions dedicated to watch the Sun closely, acquired an orbit inclination of 80 deg while retaining a perihelion radius larger than 1 AU. The spacecraft left the Earth with a staggering speed of 11.3 km/s, making it, at that time, the fastest interplanetary spacecraft ever launched. Such a high speed

was the price to be paid to reach Jupiter and pump up there the inclination for free, which also forced the orbit aphelion to be at roughly 5 AU.

The remarkably high values of ΔV that characterize space missions (also referred to as "high energy" missions) toward the circumsolar space, usually require a high hyperbolic excess velocity at launch and multiple gravity assist maneuvers to reduce the propellant consumption within acceptable limits. For example, the Solar Probe Plus [3] mission plans seven flybys with Venus, while the Solar Orbiter [2] mission schedules two flybys with Earth in addition to several Venus gravity assists.

Clearly, the presence of multiple flybys makes the transfer trajectory design more difficult and introduces constraints on the launch windows. On the other side, a direct transfer, which could offer a higher flexibility on launch windows, would be impossible for a (chemical) high thrust propulsion system, due to an excessively high value of ΔV. Not surprisingly, missions toward the heliosphere have been studied using innovative propulsion systems like solar sails [4,5,6]. Indeed solar sails are particulary suitable for transfers in the inner solar system as the propulsive force they generate is proportional to the local solar flux, which in turns varies with the inverse square distance from the Sun. Note that, in a solar-powered spacecraft in which the electric power is supplied by solar arrays, the maximum input power (and then the propulsive thrust) is an involved function of the distance from the Sun [7,8], but also depends on the flight time due to the solar cells degradation [9,10].

However, despite the recent successes of the Japanese IKAROS mission [11], which first used a solar sail for an interplanetary mission, this kind of propulsion system does not yet offer a satisfactory technology readiness level [12,13]. A possible alternative, which currently guarantees a greater confidence level, is given by solar electric propulsion (SEP) technology [14,15]. As is well known [16], the high specific impulse provided by SEP systems allows for a significant reduction of the propellant necessary to complete the transfer. Current space missions designed

to reach the inner part of the solar system with SEP technology, use SEP propulsion in combination with multiple gravity assists to maximize the payload mass delivered into the final operational orbit. Examples are the initial design of the Solar Orbiter mission [17] or the design of the BepiColombo mission [18,19]. Furthermore, future concepts envisage the use of these propulsion systems in conjunction with a solar sail, thus constituting a hybrid solution [20,21] that seeks to overcome the intrinsic limitations of the each system alone.

In any case, an assessment of the performance of a pure SEP system for a direct transfer is useful to evaluate the possible improvements provided by a hybrid solution, or by the inclusion of gravity assist maneuvers. This paper addresses a preliminary performance investigation for a spacecraft equipped with a SEP propulsion system, whose aim is to reach the circumsolar space. The study takes into account the actual performance of a SEP system of last generation. Minimum time trajectories necessary to obtain a direct transfer toward a target orbit with prescribed characteristics are found using an indirect approach based on optimal control theory. The rationale is that a minimum time trajectory provides an upper limit on the propellant mass along a possible optimal time vs. mass trade-off curve for a direct transfer. In other words any other optimal direct transfer solution that aims at minimizing the mass of propellant will have a longer transfer time.

2 Problem Description and Simulations Results

Assume that the spacecraft, with an initial in-flight mass m_0, is equipped with a solar electric propulsion system, whose performance model is based on that of NASA's Evolutionary Xenon Thruster (NEXT) [22,23]. The problem is to find the minimum time, direct trajectory (that is, without gravity assist maneuvers) that transfers the spacecraft from an Earth's heliocentric orbit to a Keplerian target orbit, under the assumption that perihelion radius r_p, aphelion radius r_a and orbital inclination i_1, are all given. The problem is solved by means of an indirect

approach using the classical calculus of variations [24,25]. The corresponding mathematical model, which is summarized in Appendix A together with the adopted nomenclature, is derived from that presented in Ref. [26]. Note that, in all of the simulations, the initial ν_0 and final ν_1 spacecraft true anomaly, the final spacecraft mass m_1, the target orbit's argument of perihelion ω_1 and the right ascension of the ascending node Ω_1, are all left free. Their optimal values are therefore obtained as outputs of the optimization process.

For a given target orbit characteristics, that is, for a given set of values (r_p, r_a, i_1), the minimum flight time t_1 is a function of both the initial spacecraft mass m_0 and the initial solar array output power $P_\oplus$ (see Appendix A for a definition of $P_\oplus$). Equivalently, in mathematical terms, the flight time may be expressed as $t_1 = t_1\,(r_p,\, r_a,\, i_1,\, m_0,\, P_\oplus)$.
For example, assume that $m_0 = 1000\,\text{kg}$, $P_\oplus = 10\,\text{kW}$, and that the target orbit characteristics are $r_p = 0.3\,\text{AU}$, $r_a = 0.8\,\text{AU}$ and $i_1 = 24\,\text{deg}$. These data are consistent with the Solar Orbiter (SOLO) working orbit [2]. The optimization process provides a minimum flight time $t_1 = 952.9\,\text{days}$, whereas the propellant consumption is $m_p \triangleq m_0 - m_1 \simeq 436.3\,\text{kg}$ (the propellant mass fraction is $m_p/m_0 = 43.6\%$). The corresponding transfer trajectory is shown in Fig. 1, where the asterisk denotes the perihelion of the parking and target orbit, whereas the circle refers to the starting (or arrival) point.

The transfer starts when the spacecraft initial true anomaly is $\nu_0 \simeq 136\,\text{deg}$, as is shown in Fig.1(a), and ~~it~~ ends when the spacecraft completes approximately four revolutions around the Sun. Note that the departure orbit coincides, by construction, with the Earth's heliocentric orbit (see Eq. (A.10)), and therefore an optimal launch window opens (yearly) on May 20.

Figure 2 shows the variation, with the orbital inclination i, of the perihelion $[p/(1+e)]$ and aphelion $[p/(1-e)]$ radius of the osculating orbit along the optimal trajectory. In particular, the figure shows that the orbital inclination varies with continuity during whole transfer but experience a steep variation when the spacecraft at the nodes. Unlike a locally optimal steering

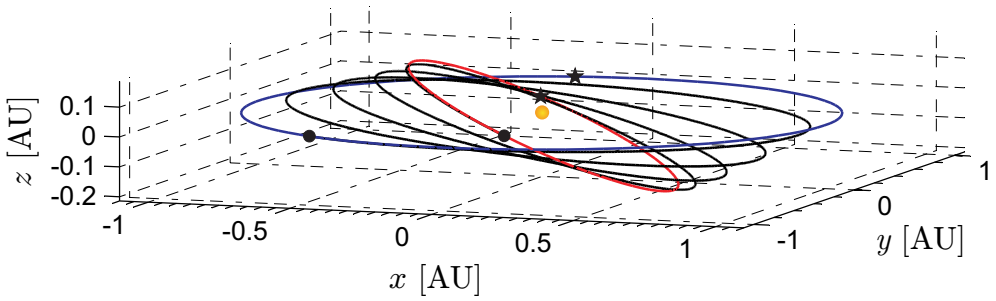

(a) Three-dimensional view.

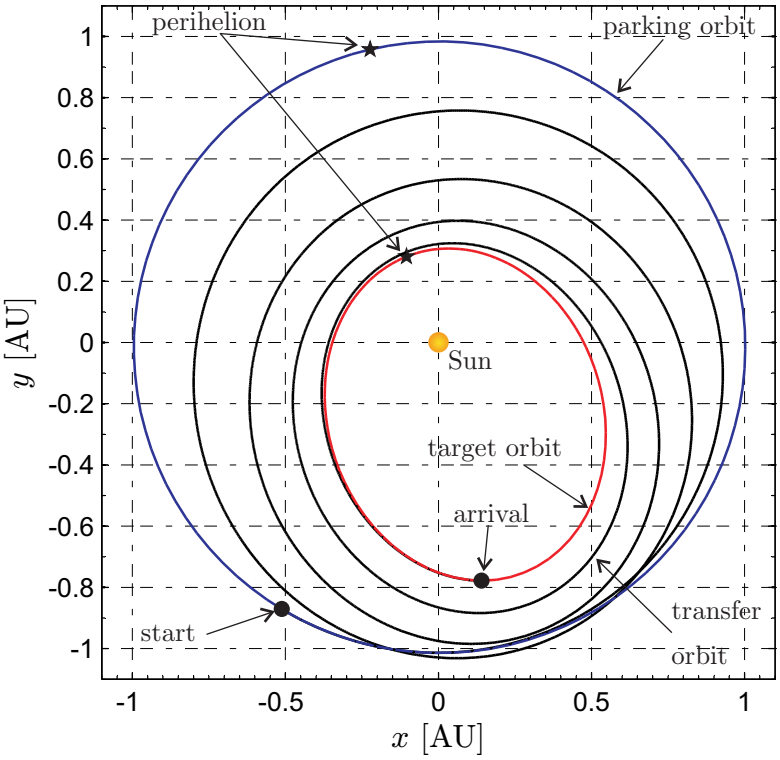

(b) Ecliptic projection.

Figure 1. Optimal transfer trajectory when $m_0 = 1000\,\mathrm{kg}$, $P_\oplus = 10\,\mathrm{kW}$, $r_p = 0.3\,\mathrm{AU}$, $r_a = 0.8\,\mathrm{AU}$, **and** $i_1 = 24\,\mathrm{deg}$.

laws [27,28], a variation of all the orbital elements to optimize the performance index (in this case the flight time) is typical of truly optimal control laws. Such a behavior is consistent with what was observed by Dachwald [5] in a similar mission scenario in which a near-term solar sail [29] reaches an heliocentric orbit with a low perihelion radius and a high inclination.

Figure 3 shows the time variation of the Sun-spacecraft distance r and the spacecraft (ecliptic) declination δ during the optimal transfer. Note that δ is the angle between the Sun-spacecraft

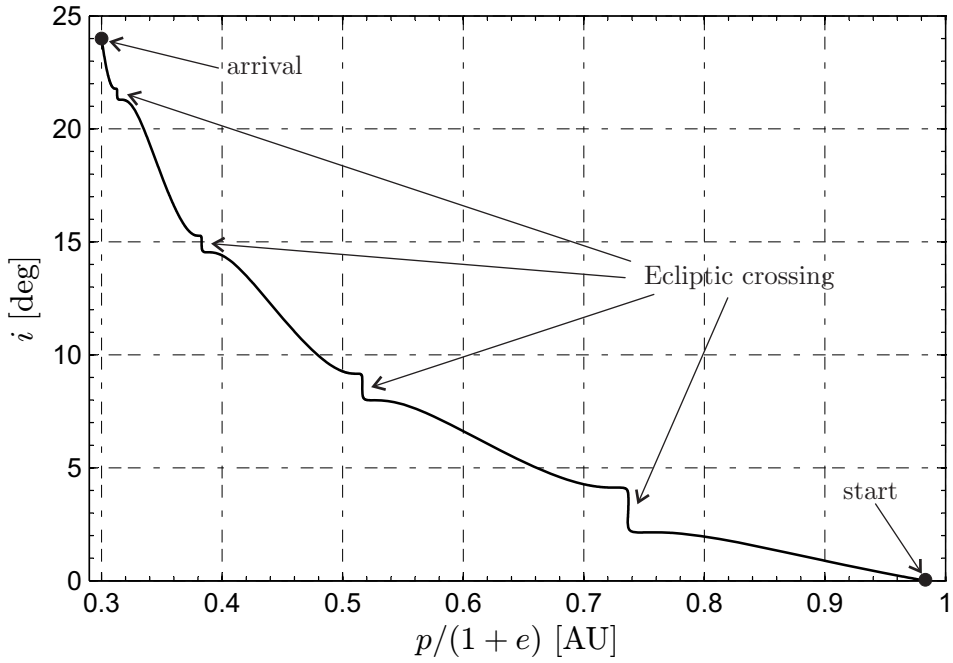

(a) Inclination vs. perihelion radius

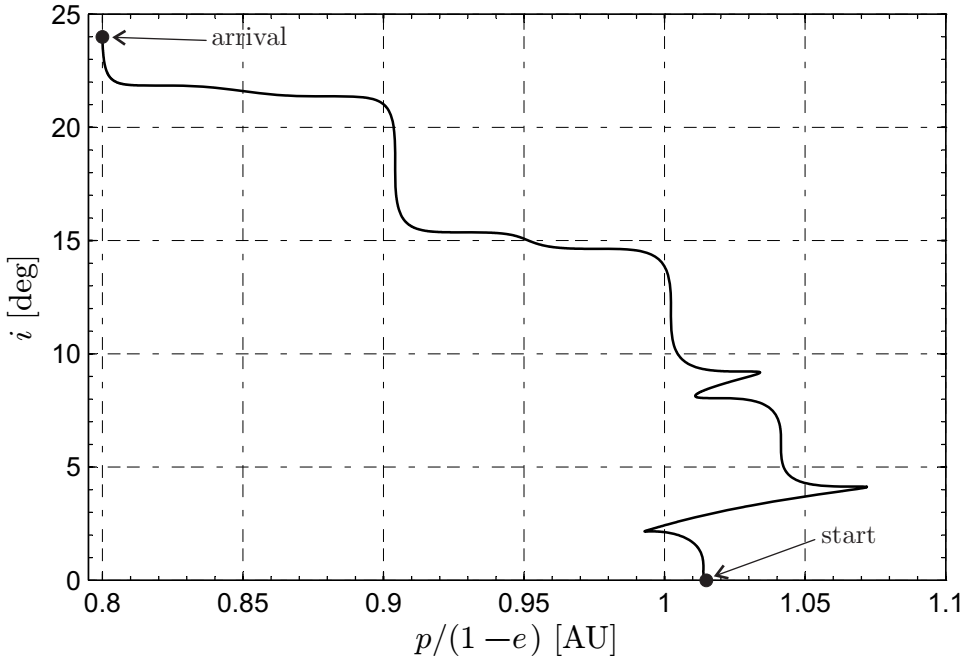

(b) Inclination vs. aphelion radius

Figure 2. Orbital inclination over perihelion and aphelion radius of the spacecraft osculating orbit (with $m_0 = 1000\,\mathrm{kg}$ and $P_\oplus = 10\,\mathrm{kW}$).

line and the Ecliptic plane. Note that the local minima of r are all located in the neighboring of the Ecliptic plane ($\delta = 0$).

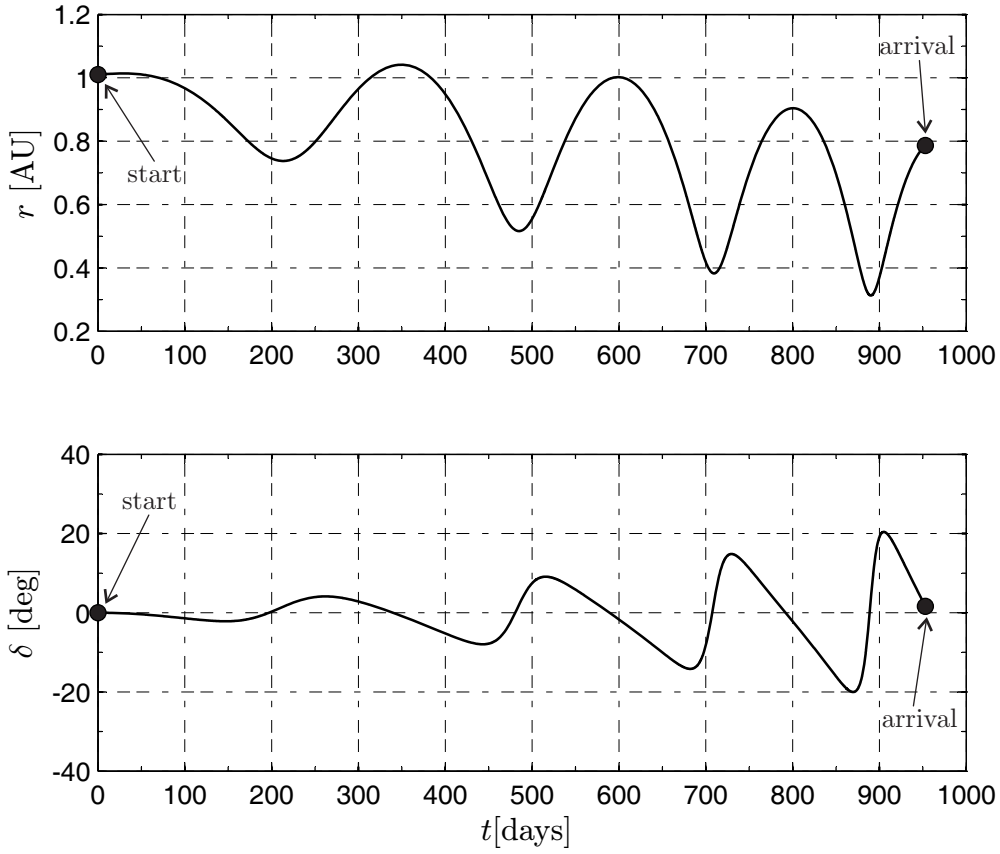

Figure 3. Sun-spacecraft distance r and ecliptic declination δ vs. time (with $m_0 = 1000\,\mathrm{kg}$, $P_\oplus = 10\,\mathrm{kW}$, $r_p = 0.3\,\mathrm{AU}$, and $r_a = 0.8\,\mathrm{AU}$).

2.1 Sensitivity analysis

A sensitivity analysis of mission performance, obtained by varying the initial spacecraft mass in the range $m_0 \in [550,\, 1350]\,\mathrm{kg}$ and the initial solar array output power in the interval $P_\oplus \in [5.5,\, 10]\,\mathrm{kW}$, is now presented. Note that a variation of $P_\oplus$ with respect to the reference value (of 10 kilowatts) may reasonably be used to model a (partial) failure of the solar electric power system. The simulation results are summarized in Tables 1 and 2, whereas the corresponding trajectories are shown in Figures 4 and 5. When the initial electric power $P_\oplus$ is kept fixed,

and initial mass m_0 is varied within the selected range, the propellant mass fraction displays a small fluctuation around a mean value of about 43.21%, see the third column of Table 1. This corresponds roughly to a linear variation of the propellant mass m_p versus the spacecraft initial mass, in the selected range. A similar conclusion holds true for the minimum flight time t_1 versus m_0, which may be approximated as

$$t_1 \simeq 0.9479\, m_0 \tag{1}$$

where t_1 is expressed in days and m_0 in kilograms.

Note that the propellant throughput capability of a NEXT propulsion system [30] is about 450 kg (qualification-level), which corresponds to 22000 hours of operation at maximum thrust (operation point $I_d = 1$, see Fig. A.1). Therefore, according to Table 1, only the mission scenario in which $m_0 \leq 1050$ kg is consistent with the actual characteristics of a single propulsive unit. However, laboratory tests [31,32] indicate that the NEXT thruster could (potentially) provide a propellant throughput greater than 750 kg, and this enhanced capability would make other mission scenarios possible.

For a given initial spacecraft mass m_0, the propellant mass fraction m_p/m_0 is strongly affected by the value of $P_\oplus$, see the third column of Table 2. This behavior is closely related to the propulsion system mathematical model described in Appendix A. In fact, as the simulations show, the optimal thrusting strategy consists of selecting (at any time) the maximum propulsive thrust. If the available power is always greater than 7.22 kW, then the thruster operation point is $I_d = 1$ along the whole transfer trajectory. This explains why a initial power $P_\oplus \geq 9.5$ kW gives the same mission performance, see the last two rows in Table 2. However, when the available power becomes less than 7.22 kW, because either the spacecraft is too far from the Sun or the value of $P_\oplus$ is insufficient, the optimization process selects an operation point different from $I_d = 1$. This situation is illustrated in Figure 6, where the time history of the

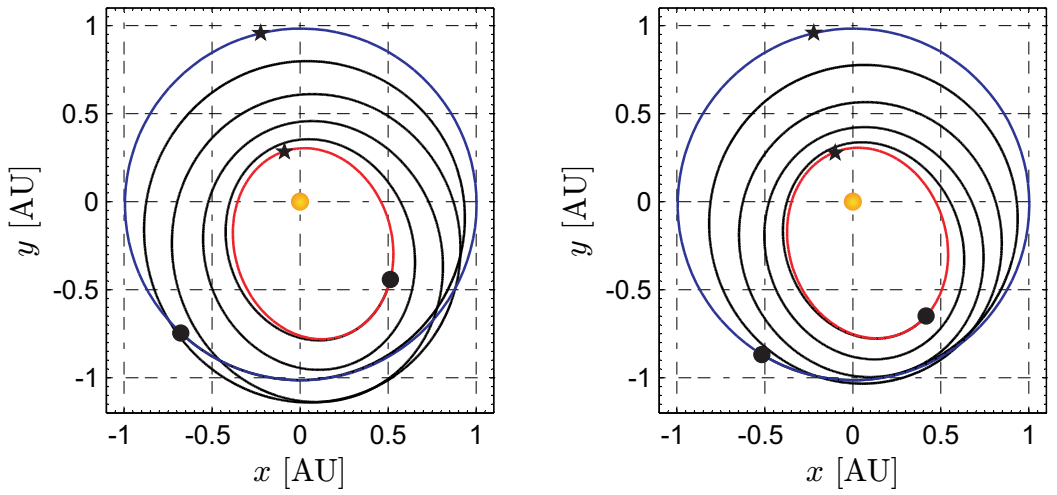

(a) $m_0 = 600\,\mathrm{kg}$.

(b) $m_0 = 700\,\mathrm{kg}$.

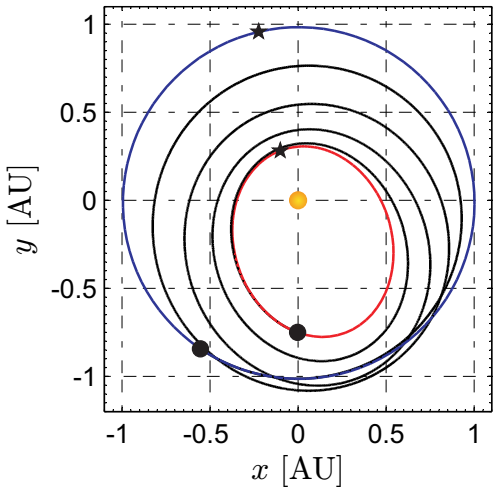

(c) $m_0 = 800\,\mathrm{kg}$.

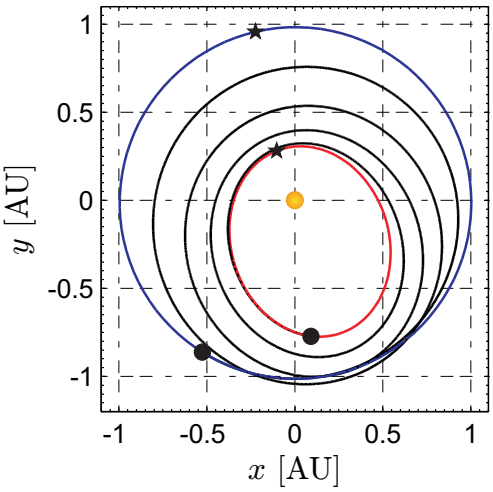

(d) $m_0 = 900\,\mathrm{kg}$.

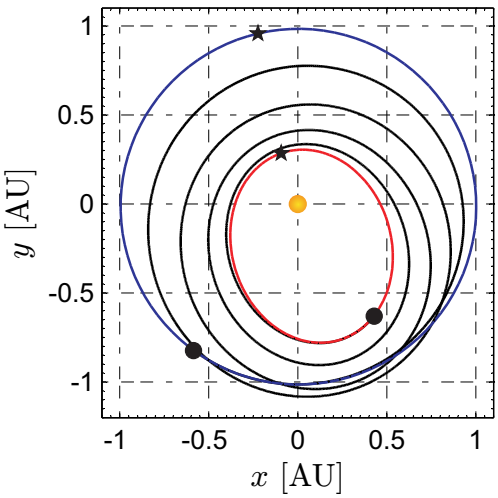

(e) $m_0 = 1100\,\mathrm{kg}$.

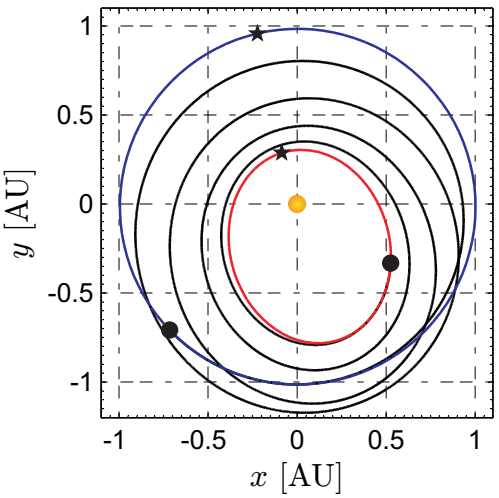

(f) $m_0 = 1200\,\mathrm{kg}$.

Figure 4. Ecliptic projection of the optimal transfer trajectory as a function of the initial mass m_0 (with $P_\oplus = 10\,\mathrm{kW}$, $r_p = 0.3\,\mathrm{AU}$, $r_a = 0.8\,\mathrm{AU}$, and $i_1 = 24\,\mathrm{deg}$).

m_0 [kg]	t_1 [days]	m_p/m_0	m_p [kg]
550	509.7	0.4243	233.3
600	550.2	0.4198	251.9
650	601.7	0.4239	275.5
700	658.6	0.4308	301.5
750	712.8	0.4351	326.3
800	749.9	0.4292	343.4
850	793.2	0.4273	363.2
900	843.4	0.4291	386.1
950	902.9	0.4351	413.4
1000	952.9	0.4363	436.2
1050	998.1	0.4352	457.0
1100	1031.2	0.4292	472.1
1150	1080.7	0.4303	494.8
1200	1135.6	0.4333	519.9
1250	1187.0	0.4348	543.5
1300	1240.1	0.4368	567.7
1350	1307.4	0.4434	598.6
1400	1319.2	0.4314	604
1450	1371.7	0.4331	628.1
1500	1432.8	0.4373	656
1600	1511.1	0.4324	691.8
1700	1612.4	0.4342	738.3
1800	1720	0.4375	787.5

Table 1
Mission performance as a function of the initial spacecraft mass m_0 (with $P_\oplus = 10\,\mathrm{kW}$, $r_p = 0.3\,\mathrm{AU}$, $r_a = 0.8\,\mathrm{AU}$, and $i_1 = 24\,\mathrm{deg}$).

thruster operation point I_d is shown as a function of $P_\oplus$.

The flight time and the propellant mass fraction depend on the target orbit characteristics. For example Tables 3 and 4 show the mission performance as a function of $i_1 \in [0,\, 50]\,\mathrm{deg}$ and $r_a \in [0.3,\, 1]\,\mathrm{AU}$, respectively. Note that the case of $i_1 = 0$ corresponds to a two-dimensional transfer towards an elliptic target orbit with perihelion radius $r_p = 0.3\,\mathrm{AU}$ and aphelion radius $r_a = 0.8\,\mathrm{AU}$. The case of $r_a = 0.3\,\mathrm{AU}$, instead, corresponds to an optimal transfer towards a circular heliocentric orbit with inclination $i_1 = 24\,\mathrm{deg}$, see Fig. 7.

$P_\oplus$ [kW]	t_1 [days]	m_p/m_0
5.5	1278.6	0.5125
6	1134.7	0.4895
6.5	1044.6	0.4713
7	1004.6	0.46
7.5	1003	0.4592
8	987.2	0.4520
8.5	964.8	0.4418
9	959.7	0.4394
9.5	952.9	0.4363
10	952.9	0.4363

Table 2
Mission performance as a function of the initial solar array initial output power $P_\oplus$ (with $m_0 = 1000\,\mathrm{kg}$, $r_p = 0.3\,\mathrm{AU}$, $r_a = 0.8\,\mathrm{AU}$, and $i_1 = 24\,\mathrm{deg}$).

i_1 [deg]	t_1 [days]	m_p/m_0
0	673.4	0.3083
5	693.6	0.3176
10	732.9	0.3355
15	788.3	0.3609
20	873.9	0.4001
25	965.8	0.4422
30	1052.8	0.4820
35	1128.4	0.5166
40	1251.2	0.5578
50	1583.5	0.6367

Table 3
Mission performance as a function of i_1 (with $m_0 = 1000\,\mathrm{kg}$, $P_\oplus = 10\,\mathrm{kW}$, $r_p = 0.3\,\mathrm{AU}$, and $r_a = 0.8\,\mathrm{AU}$).

3 Conclusions

The design of high-energy space physics missions offer the intriguing opportunity to explore the capabilities of both advanced electric propulsion concepts and optimization algorithms. This paper thoroughly investigates minimum time optimal transfer scenarios for a mission to

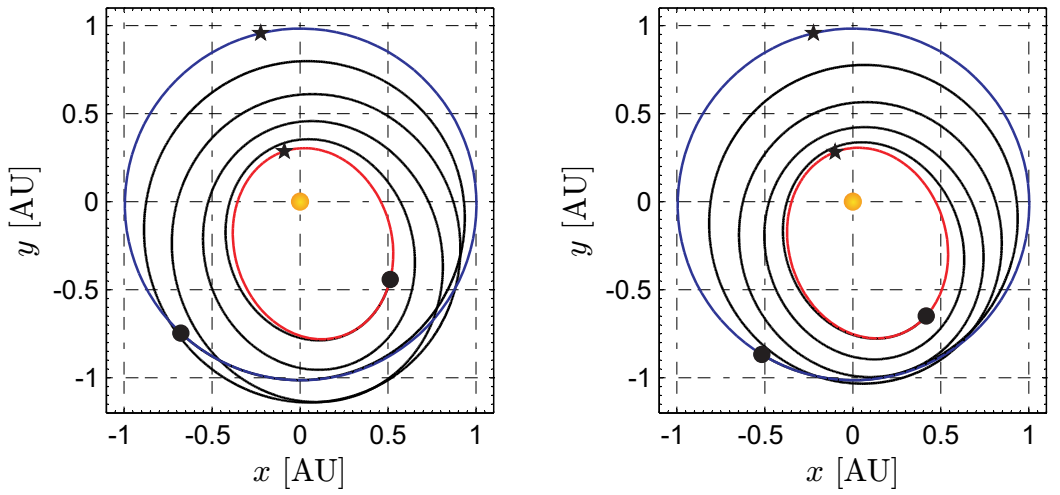

(a) $P_{\oplus} = 6\,\mathrm{kW}$.

(b) $P_{\oplus} = 7\,\mathrm{kW}$.

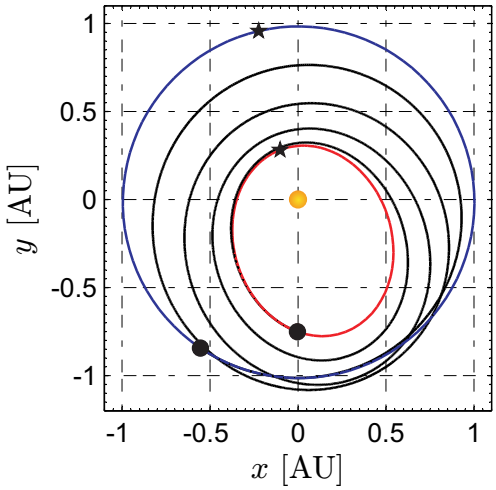

(c) $P_{\oplus} = 8\,\mathrm{kW}$.

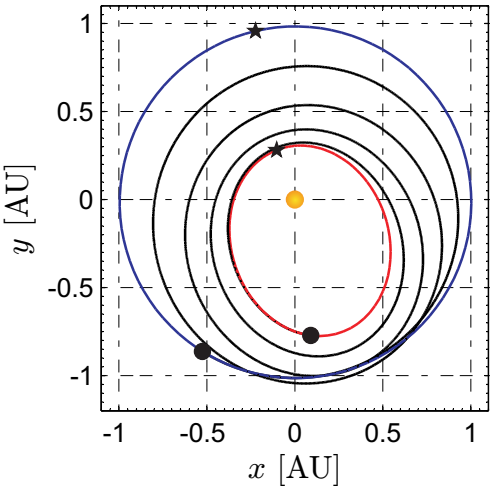

(d) $P_{\oplus} = 9\,\mathrm{kW}$.

Figure 5. Ecliptic projection of the optimal transfer trajectory as a function of the initial solar array output power $P_{\oplus}$ (with $m_0 = 1000\,\mathrm{kg}$, $r_p = 0.3\,\mathrm{AU}$, $r_a = 0.8\,\mathrm{AU}$, and $i_1 = 24\,\mathrm{deg}$).

the circumsolar space, in which a solar electric propelled spacecraft enters an elliptical highly inclined orbit around the Sun with a perihelion radius of 0.3 AU (about 65 solar radii).

Using an indirect approach, a number of time-optimal (direct) transfer trajectories have been simulated, and the resulting data have been collected in graphs and tables for a trade-off analysis of the main mission parameters. Taking into account the actual performance of an advanced electric propulsion system (the NASA Evolutionary Xenon Thruster), the simula-

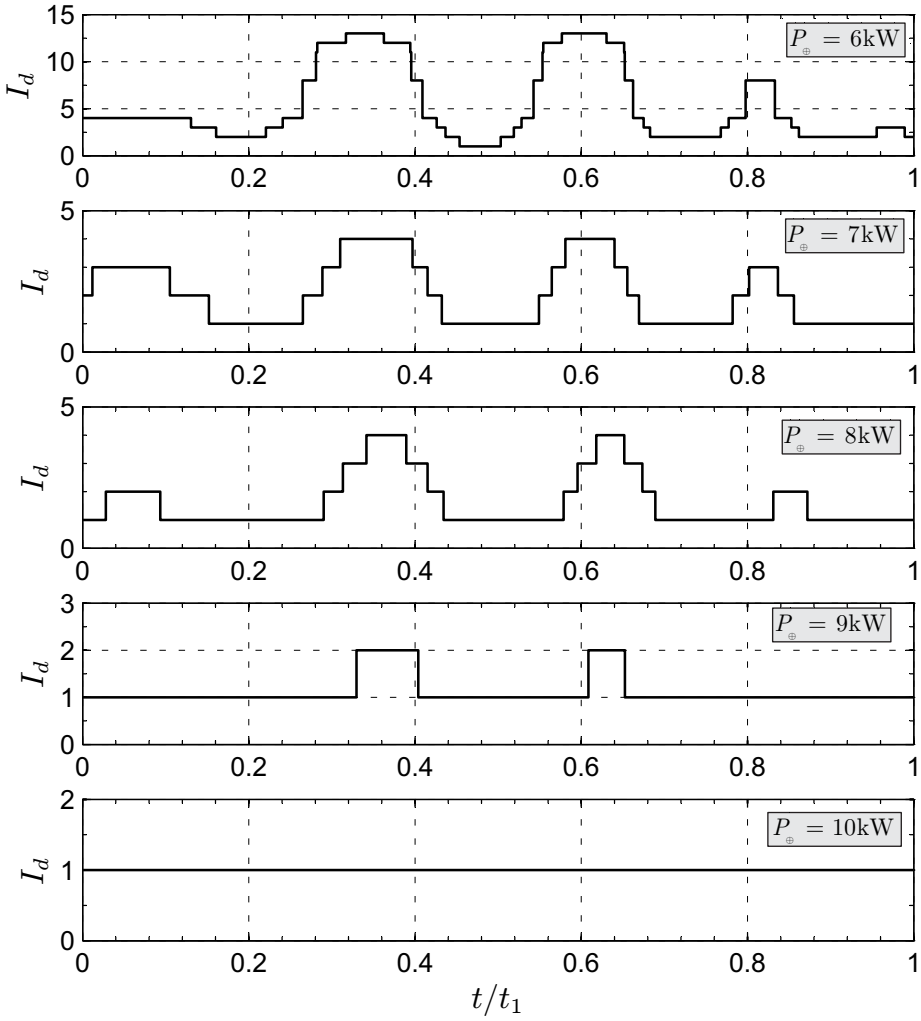

Figure 6. Thruster operation point I_d vs. time as a function of the initial solar array output power $P_\oplus$ (with $m_0 = 1000\,\mathrm{kg}$, $r_p = 0.3\,\mathrm{AU}$, $r_a = 0.8\,\mathrm{AU}$, and $i_1 = 24\,\mathrm{deg}$).

tions show that a spacecraft with an initial mass of 1000 kg reaches a target orbit of inclination 24 deg and aphelion radius 0.8 AU in about 2.6 years. In this mission scenario, the final spacecraft's mass is slightly greater than the 56% of the initial in-flight mass. This rather small value could be increased, at the expense of an increased flight time, by including, in the performance index, a term depending on the final spacecraft's mass. On the other hands, a transfer trajectory that minimizes only the propellant consumption, should be time-constrained. Therefore, the results of the minimum-time problem ensure that the time-constraint in a fuel-optimal problem is feasible. The use of optimal control theory has provided an optimal switching law for the operation point of the engine showing substantially different behaviors depending on

r_a [AU]	t_1 [days]	m_p/m_0
0.3	1240	0.5679
0.4	1151.5	0.5272
0.5	1078.6	0.4938
0.6	1018.8	0.4665
0.7	969.7	0.444
0.8	952.9	0.4363
0.9	914.5	0.4187
1	893.5	0.4091

Table 4
Mission performance as a function of r_a (with $m_0 = 1000\,\mathrm{kg}$, $P_\oplus = 10\,\mathrm{kW}$, $r_p = 0.3\,\mathrm{AU}$, and $i_1 = 24\,\mathrm{deg}$).

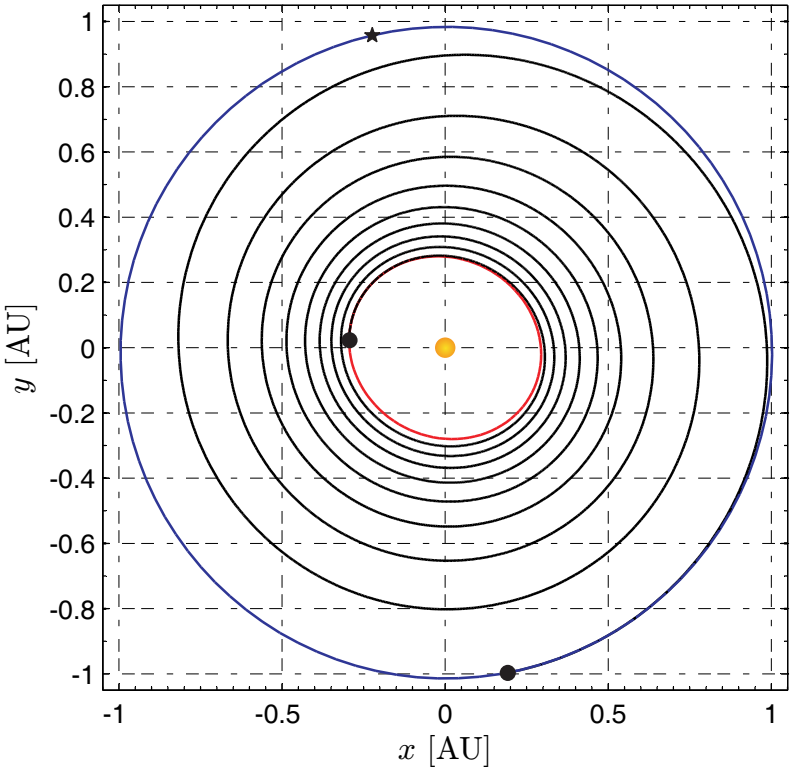

Figure 7. Ecliptic projection of the optimal transfer trajectory when $m_0 = 1000\,\mathrm{kg}$, $P_\oplus = 10\,\mathrm{kW}$, $r_p \equiv r_a = 0.3\,\mathrm{AU}$, and $i_1 = 24\,\mathrm{deg}$.

the available power. This situation can correspond to an intentionally undersized power system or to a partial failure.

A natural extension of the analysis discussed in this paper, is to include one or more gravity-

assist maneuvers, whose aim is tho reduce the propellant consumption, as in the case of the ESA's Solar Orbiter mission study. However, a multiple gravity assist trajectory places additional constraints related to the planetary ephemerides, whereas a direct transfer offers a greater flexibility.

A Mathematical Model

The equations of motion [33,26] of a solar electric propelled spacecraft, in a heliocentric inertial reference frame, may be expressed in terms of Modified Equinoctial Orbital Elements [34,35] (MEOE) p, f, g, h, k, and L as:

$$\dot{\boldsymbol{x}} = \eta_P \, (T/m) \, \mathbb{A} \, \hat{\boldsymbol{a}}_T + \boldsymbol{d} \tag{A.1}$$

where $\boldsymbol{x} \triangleq [p,\, f,\, g,\, h,\, k,\, L, m]^{\mathrm{T}}$ is the state vector, m is the spacecraft mass, $T \geq 0$ is the propulsive thrust modulus, $\hat{\boldsymbol{a}}_T$ is the thrust unit vector, and $\eta_P = 0.92$ is the duty cycle. The latter, according to Rayman and Williams [8], is the fraction of time during deterministic

thrust periods in which $T \neq 0$. In Eq. (A.1), $\mathbb{A} \in \mathbb{R}^{7\times 3}$ is a matrix in the form:

$$\mathbb{A} \triangleq \sqrt{\frac{p}{\mu_\odot}} \begin{bmatrix} 0 & \left[\dfrac{2\,p}{1+f\,\cos L+g\,\sin L}\right] & 0 \\ [\sin L] & \left[\dfrac{(2+f\,\cos L+g\,\sin L)\,\cos L+f}{1+f\,\cos L+g\,\sin L}\right] & \left[-\dfrac{g\,(h\,\sin L-k\,\cos L)}{1+f\,\cos L+g\,\sin L}\right] \\ [-\cos L] & \left[\dfrac{(2+f\,\cos L+g\,\sin L)\,\sin L+g}{1+f\,\cos L+g\,\sin L}\right] & \left[\dfrac{f\,(h\,\sin L-k\,\cos L)}{1+f\,\cos L+g\,\sin L}\right] \\ 0 & 0 & \left[\dfrac{(1+h^2+k^2)\,\cos L}{2\,(1+f\,\cos L+g\,\sin L)}\right] \\ 0 & 0 & \left[\dfrac{(1+h^2+k^2)\,\sin L}{2\,(1+f\,\cos L+g\,\sin L)}\right] \\ 0 & 0 & \left[\dfrac{h\,\sin L-k\,\cos L}{1+f\,\cos L+g\,\sin L}\right] \\ 0 & 0 & 0 \end{bmatrix} \tag{A.2}$$

where $\mu_\odot = 132\,712\,439\,935.5\,\mathrm{km}^3/\mathrm{s}^2$ is the Sun's gravitational parameter, and the vector $\boldsymbol{d} \in \mathbb{R}^{7\times 1}$ is defined as

$$\boldsymbol{d} \triangleq \left[0,\,0,\,0,\,0,\,0,\,\sqrt{\mu_\odot\,p}\,\left(\frac{1+f\,\cos L+g\,\sin L}{p}\right)^2,\,-\eta_P\,\beta\right]^{\mathrm{T}} \tag{A.3}$$

where $\beta \geq 0$ is the propellant mass flow rate. Note that p is the semilatus rectum of the spacecraft osculating orbit, whereas the transformations from MEOE to the classical orbital

elements are

$$a = \frac{p}{1 - f^2 - g^2} \tag{A.4}$$

$$e = \sqrt{f^2 + g^2} \tag{A.5}$$

$$i = 2 \arctan \sqrt{h^2 + k^2} \tag{A.6}$$

$$\sin \omega = g\, h - f\, k \quad , \quad \cos \omega = f\, h + g\, k \tag{A.7}$$

$$\sin \Omega = k \quad , \quad \cos \Omega = h \tag{A.8}$$

$$\nu = L - \Omega - \omega \tag{A.9}$$

where a is the semimajor axis, e is the eccentricity, i the orbital inclination, ω is the argument of perihelion, Ω is the longitude of the ascending node, and ν is the true anomaly.

In a solar electric propelled spacecraft, the thrust level and the propellant mass flow rate are closely related to the input power P to the Power Processing Unit (PPU). In particular, an electric thruster has a finite number of operation points [22,23], each one characterized by a corresponding set of values of T, β, and P. If the propulsion system performance coincides with that of a NEXT ion thruster, a set of 40 operation points (or I_d) is available [23], see Fig. A.1. In the simulations, a fictitious operation point (that is $I_d = 41$, where $T = 0$ and $\beta = 0$) has been added to the actual NEXT thrust table, to model the presence of possible coasting phases in the spacecraft optimal trajectory. Therefore, within this simplified model, the operation point $I_d \in \mathbb{N}^+$ (with $I_d \leq 41$), represents the only control parameter that describes the thruster performance in terms of T and β.

For example, when the first operation point $I_d = 1$ is selected, the propulsion system supplies the maximum thrust (about 0.236 N) at the maximum propellant mass flow rate (about 5.76 mg/s), see Fig. A.1. Note that the condition $I_d = 1$ can be selected only if the PPU input

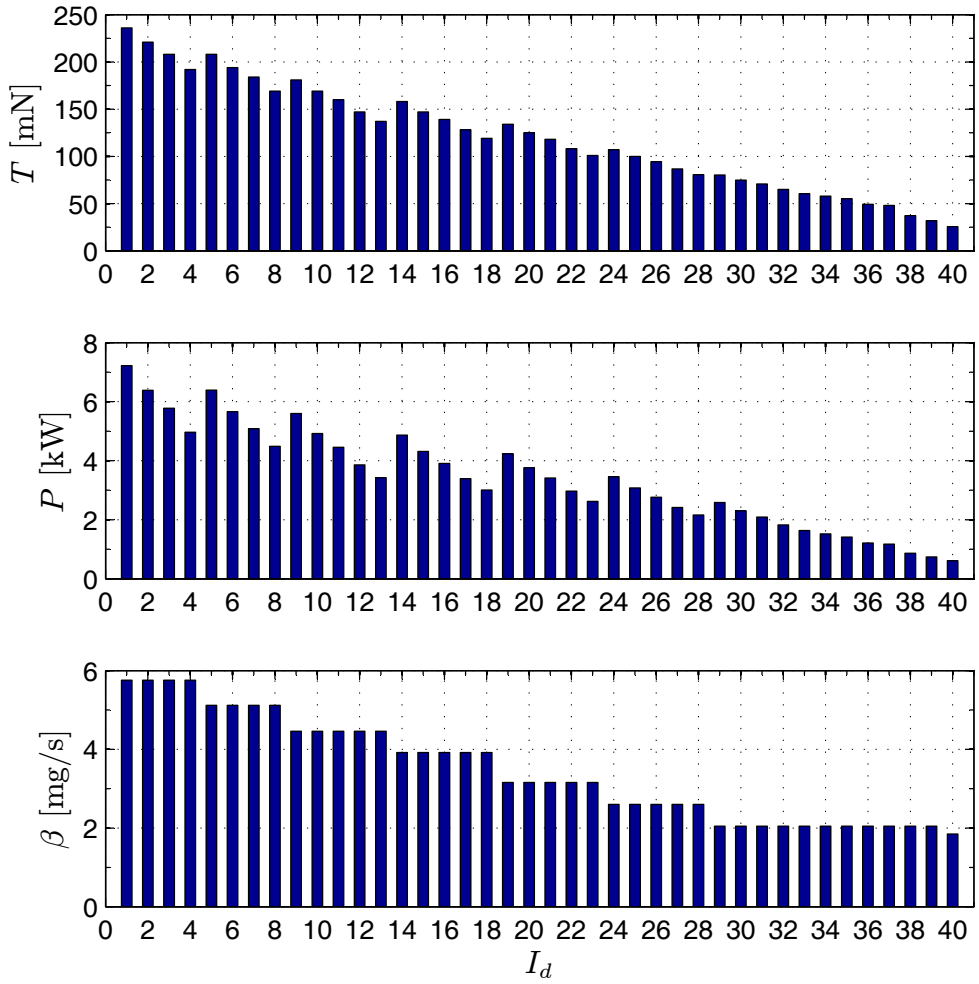

Figure A.1. Propulsion system operation points in terms of thrust T, propellant mass flow rate β, and PPU input power P (data adapted from Ref. [23]).

power is (at least) 7.22 kW. In fact, assuming a photovoltaic power generation system with degradation effects [8,36], the set of all admissible operation points is strictly related to the available input power. The latter is defined as the difference of the solar array output power and the power allocated to operate the spacecraft systems $P_L \triangleq 400\,\mathrm{W}$. Therefore, when an initial output power $P_\oplus$ is given, the set of admissible operation points depends both on the spacecraft-Sun distance and the time [8]. The mathematical model and the flow diagram of the electric power calculation are discussed in Ref. [26]. In this paper $P_\oplus$ is chosen to coincide with the solar array output power at the beginning of the mission at a reference Sun-spacecraft distance equal to 1 AU.

A.1 Trajectory optimization

Assume that the initial (corresponding to $t_0 \triangleq 0$) spacecraft osculating orbit coincides with the Earth's (Keplerian) heliocentric orbit, viz.

$$p(t_0) = 9.9878 \times 10^{-1}\,\mathrm{AU} \quad , \quad f(t_0) = -3.5778 \times 10^{-3} \quad , \quad g(t_0) = 1.5344 \times 10^{-2}$$
$$h(t_0) = -1.5181 \times 10^{-5} \quad , \quad k(t_0) = 2.1250 \times 10^{-5} \tag{A.10}$$

This scenario is representative of a spacecraft injection on a parabolic Earth escape trajectory, with zero hyperbolic excess energy with respect to the planet.

The optimization problem consists of finding the minimum time trajectory that transfers the spacecraft from the initial orbit to a final (prescribed) target orbit. This amounts to maximizing the objective function $J \triangleq -t_1$, where t_1 is the total flight time. Using an indirect approach [25], the optimal thrust direction $\hat{\boldsymbol{a}}_T$ is obtained through Pontryagin's maximum principle [37,38] as

$$\hat{\boldsymbol{a}}_T = \frac{\mathbb{A}^{\mathrm{T}}\,\boldsymbol{\lambda}}{\|\mathbb{A}^{\mathrm{T}}\,\boldsymbol{\lambda}\|} \tag{A.11}$$

where $\boldsymbol{\lambda} \in \mathbb{R}^{7\times 1}$ is the adjoint vector

$$\boldsymbol{\lambda} \triangleq [\lambda_p,\, \lambda_f,\, \lambda_g,\, \lambda_h,\, \lambda_k,\, \lambda_L,\, \lambda_m]^{\mathrm{T}} \tag{A.12}$$

whose time derivative is given by the Euler-Lagrange equations $\dot{\boldsymbol{\lambda}} = -\partial H/\partial \boldsymbol{x}$ where $H \triangleq [\eta_P\,(T/m)\,\mathbb{A}\,\hat{\boldsymbol{a}}_T \cdot \boldsymbol{\lambda} + \boldsymbol{d} \cdot \boldsymbol{\lambda}]$ is the Hamiltonian function. According to Ref. [26], the optimal thrust level T (and so the propellant mass flow rate β) is obtained, using a numerical approach [39], by maximizing the Hamiltonian H with respect to I_d. Note that the maximization process of H should take into account the constraint condition on the actual value of the available power for the propulsion system.

The spacecraft motion is described by the seven equations of motion (A.1) and the seven Euler-Lagrange equations. This differential system must be completed with 14 suitable boundary conditions, the first five of these are shown in Eq. (A.10). Because the initial spacecraft angular position is left free, the initial true longitude $L(t_0)$ is an output of the optimization process. The sixth boundary condition refers to the initial (given) spacecraft mass $m_0 \triangleq m(t_0)$, whereas the remaining eight conditions (along with the minimum flight time t_1) are obtained by enforcing the transversality condition [24], following the procedure described in Refs. [40,41]. Note that, when the inclination i_1, the perihelion radius r_p, and the aphelion radius r_a of the heliocentric target orbit are all fixed, Eqs. (A.5) and (A.6) provide the following three constraints on the final value (subscript 1) of MEOE:

$$i_1 = 2 \arctan\sqrt{h_1^2 + k_1^2} \quad , \quad \frac{r_a - r_p}{r_a + r_p} = \sqrt{f_1^2 + g_1^2} \quad , \quad p_1 = \frac{2\, r_p\, r_a}{r_p + r_a} \tag{A.13}$$

A set of heliocentric canonical units [42], in which the spacecraft initial in-flight mass m_0 coincides with the mass unit, has been used in the integration of the differential equations to reduce their numerical sensitivity. The equations of motion and the Euler-Lagrange equations have been integrated in double precision using a variable order Adams-Bashforth-Moulton solver scheme [43,44] with absolute and relative errors of 10^{-12}. Finally, the boundary-value problem associated to the variational problem has been solved through a hybrid numerical technique that combines genetic algorithms (to obtain a first estimate of adjoint variables), with gradient-based and direct methods to refine the solution.

Acknowledgments

The authors would like to acknowledge the valuable support and suggestions by Prof. Giovanni Mengali from University of Pisa, and Prof. Lorenzo Casalino from Politecnico di Torino.

References

[1] Heliophysics Roadmap Team, Heliophysics/solar & space physics of a new era: Recommended roadmap for science and technology 2009–2030, Report to the NASA Advisory Council Heliophysics Subcommittee, NASA, available online (cited February 23, 2012) `http://sec.gsfc.nasa.gov/2009_Roadmap.pdf` (May 2009).

[2] ESA Study Scientists, Solar orbiter: Exploring the sun-heliosphere connection, Definition Study Report ESA/SRE(2011)14, European Space Agency, available online (cited February 4, 2012) `http://sci.esa.int/science-e/www/object/index.cfm?fobjectid=48985` (July, 25 2011).

[3] APL Team, Solar Probe Plus mission engineering study report, Tech. rep., The Johns Hopkins University Applied Physics Laboratory, available online (cited February 4, 2012) `http://solarprobe.jhuapl.edu/mission/docs/SolarProbeME.pdf` (March 10 2008).

[4] C. G. Sauer, Jr., Solar sail trajectories for solar polar and interstellar probe missions, in: AAS/AIAA Astrodynamics Specialist Conference, 1999, paper AAS 99-336.

[5] B. Dachwald, A. Ohndorf, B. Wie, Solar sail trajectory optimization for the solar polar imager (SPI) mission, in: AIAA/AAS Astrodynamics Specialist Conference and Exhibit, Keystone, Colorado, 2006, paper AIAA 2006-6177.

[6] G. Mengali, A. A. Quarta, Solar sail near-optimal circular transfers with plane change, Journal of Guidance, Control, and Dynamics 32 (2) (2009) 456–463, doi: 10.2514/1.38079.

[7] C. G. Sauer, Jr., Modeling of thruster and solar array characteristics in the jpl low-thrust trajectory analysis, in: 13th International Electric Propulsion Conference, San Diego, CA, 1978, paper AIAA 78-645.

[8] M. D. Rayman, S. N. Williams, Design of the first interplanetary solar electric propulsion mission, Journal of Spacecraft and Rockets 39 (4) (2002) 589–595, doi: 10.2514/2.3848.

[9] G. G. J. Bourke, R. D. Sauer, The effect of solar array degradation on electric propulsion

spacecraft performance, in: AIAA 9th Electric Propulsion Conference, Bethesda, MD, USA, 1972, paper AIAA 72-444.

[10] J. H. Saleh, D. E. Hastings, D. J. Newman, Spacecraft design lifetime, Journal of Spacecraft and Rockets 39 (2) (2002) 244–257, doi: 10.2514/2.3806.

[11] Y. Tsuda, O. Mori, R. Funase, H. Sawada, T. Yamamoto, T. Saiki, T. Endo, J. Kawaguchi, Flight status of IKAROS deep space solar sail demonstrator, Acta Astronautica 69 (9-10) (2011) 833–840, doi: 10.1016/j.actaastro.2011.06.005.

[12] M. Macdonald, C. R. McInnes, Solar sail science mission applications and advancement, Advances in Space Research 48 (11) (2011) 1702–1716, doi: 10.1016/j.asr.2011.03.018.

[13] L. Johnson, R. Young, E. Montgomery, D. Alhorn, Status of solar sail technology within NASA, Advances in Space Research 48 (11) (2011) 1687–1694, doi: 10.1016/j.asr.2010.12.011.

[14] J. R. Brophy, M. Noca, Electric propulsion for solar system exploration, Journal of Propulsion and Power 14 (5) (1998) 700–707, doi: 10.2514/2.5332.

[15] K. Toki, H. Kuninaka, Y. Shimizu, K. Kuriki, Accomplishment and prospect of isas electric propulsion, Acta Astronautica 50 (5) (2002) 285–294, doi: 10.1016/S0094-5765(01)00177-1.

[16] S. N. Williams, V. Coverstone-Carroll, Benefits of solar electric propulsion for the next generation of planetary exploration missions, Journal of the Astronautical Sciences 45 (2) (1997) 143–159 .

[17] M. Vasile, F. Bernelli-Zazzera, Trajectory Design Combining Low-Thrust and Gravity Assist Manoeuvres, Vol. 79 of Operations Research in Space and Air, Springer, 2003, Ch. 12, pp. 1–31, ISBN: 978-1-4020-1218-1.

[18] M. Vasile, F. Bernelli-Zazzera, Optimizing low-thrust and gravity assist maneuvers to design interplanetary trajectories, The Journal of the Astronautical Sciences 51 (1) (2003) 13–35 .

[19] S. Campagnola, C. Corral, J. R., Design of lunar gravity-assist for the bepicolombo mission to mercury, in: 14th AAS/AIAA Space Flight Mechanics Conference, Maui, Hawaii, 2004, paper AAS 04-130.

[20] M. Leipold, M. Götz, Hybrid photonic/electric propulsion, Tech. Rep. SOL4-TR-KTH-0001, Kayser-Threde GmbH, Munich, Germany, ESA contract No. 15334/01/NL/PA (January 2002).

[21] G. Mengali, A. A. Quarta, Trajectory design with hybrid low-thrust propulsion system, Journal of Guidance, Control, and Dynamics 30 (2) (2007) 419–426, doi: 10.2514/1.22433.

[22] M. J. Patterson, T. W. Haag, J. E. Foster, V. K. Rawlin, R. F. Roman, G. C. Soulas, Development status of a 5/10-kW class ion engine, in: 37th AIAA/ASME/SAE/ASEE Joint Propulsion Conference and Exhibit, Salt Lake City, UT, 2001, paper AIAA 2001-3489.

[23] M. J. Patterson, S. W. Benson, NEXT ion propulsion system development status and performance, in: 43rd AIAA/ASME/SAE/ASEE Joint Propulsion Conference and Exhibit, Cincinnati, OH, 2007, paper AIAA 2007-5199.

[24] A. E. Bryson, Y. C. Ho, Applied Optimal Control, Hemisphere Publishing Corporation, New York, NY, 1975, Ch. 2, pp. 71–89, ISBN: 0-891-16228-3.

[25] J. T. Betts, Survey of numerical methods for trajectory optimization, Journal of Guidance, Control, and Dynamics 21 (2) (1998) 193–207, doi: 10.2514/2.4231.

[26] A. A. Quarta, G. Mengali, Minimum-time space missions with solar electric propulsion, Aerospace Science and Technology 15 (5) (2011) 381–392, doi: 10.1016/j.ast.2010.09.003.

[27] M. Macdonald, C. R. McInnes, Analytical control laws for planet-centered solar sailing, Journal of Guidance, Control, and Dynamics 28 (5) (2005) 1038–1048, doi: 10.2514/1.11400.

[28] M. Macdonald, C. R. McInnes, Analytic control laws for near-optimal geocentric solar sail transfers, in: AAS/AIAA Astrodynamics Specialists Conference, Quebec, Canada, 2001, paper AAS 01-472.

[29] C. R. McInnes, Near-term, low cost missions for solar sails, Journal of the British Interplanetary Society 53 (1-2) (2000) 48–61 .

[30] J. Van Noord, Lifetime assessment of the NEXT ion thruster, in: 43rd AIAA/ASME/SAE/ASEE Joint Propulsion Conference and Exhibit, Cincinnati, OH, 2007, paper AIAA 2007-5274.

[31] D. A. Herman, G. C. Soulas, M. J. Patterson, NEXT long-duration test neutralizer performance and erosion characteristics, in: The 31st International Electric Propulsion Conference, University of Michigan, USA, 2009, paper IEPC-2009-154 (Also NASA Technical Memorandum NASA/TM–2009-215838).

[32] T. A. Reckart, NASA's evolutionary xenon thruster (NEXT), NASA fact sheets, NASA, In-Space Propulsion Technology Project, John H. Glenn Research Center, Cleveland, Ohio 44135, available online (cited February 6, 2012) `http://microgravity.grc.nasa.gov/Advanced/ScienceProject/FactSheets/NEXT.pdf` (May, 22 2009).

[33] J. T. Betts, Very low-thrust trajectory optimization using a direct SQP method, Journal of Computational and Applied Mathematics 120 (1) (2000) 27–40, doi: 10.1016/S0377-0427(00)00301-0.

[34] M. J. H. Walker, J. Owens, B. Ireland, A set of modified equinoctial orbit elements, Celestial Mechanics 36 (1985) 409–419, doi: 10.1007/BF01227493.

[35] M. J. Walker, Erratum - a set of modified equinoctial orbit elements, Celestial Mechanics 38 (4) (1986) 391–392, doi: 10.1007/BF01238929.

[36] D. Y. Oh, Evaluation of solar electric propulsion technologies for discovery-class missions, Journal of Spacecraft and Rockets 44 (2) (2007) 399–411, doi: 10.2514/1.21613.

[37] V. A. Chobotov, Orbital Mechanics, 2nd Edition, AIAA Education Series, American Institute of Aeronautics and Astronautics, New York, 1996, Ch. 9, ISBN: 1-563-47179-5.

[38] J. A. Kechichian, Optimal low-thrust rendezvous using equinoctial orbit elements, Acta Astronautica 38 (1) (1996) 1 – 14, doi: 10.1016/0094-5765(95)00121-2.

[39] C. A. R. Hoare, Quicksort, The Computer Journal 5 (1) (1962) 10–16, doi: doi:10.1093/comjnl/5.1.10.

[40] L. Casalino, G. Colasurdo, D. Pastrone, Optimization procedure for preliminary design of opposition-class mars missions, Journal of Guidance, Control, and Dynamics 21 (1) (1998) 134–140, doi: 10.2514/2.4209.

[41] L. Casalino, G. Colasurdo, D. Pastrone, Optimal low-thrust escape trajectories using gravity assist, Journal of Guidance, Control, and Dynamics 22 (5) (1999) 637–642, doi: 10.2514/2.4451.

[42] R. R. Bate, D. D. Mueller, J. E. White, Fundamentals of Astrodynamics, Dover Publications, New York, 1971, p. 429, ISBN: 0-486-60061-0.

[43] L. F. Shampine, M. K. Gordon, Computer Solution of Ordinary Differential Equations: The Initial Value Problem, W. H. Freeman & Co Ltd, San Francisco, 1975, Ch. 10, ISBN: 0-716-70461-7.

[44] L. F. Shampine, M. W. Reichelt, The MATLAB ODE suite, SIAM Journal on Scientific Computing 18 (1) (1997) 1–22, doi: 10.1137/S1064827594276424.